Proton and electron transfer in bacterial reaction centers. Biochim Biophys Acta 1458: 148–163

ARTICLE *in* BIOCHIMICA ET BIOPHYSICA ACTA · JUNE 2000

Impact Factor: 4.66 · DOI: 10.1016/S0005-2728(00)00065-7 · Source: PubMed

4 AUTHORS, INCLUDING:

Melvin Y Okamura
University of California, San Diego
132 PUBLICATIONS **7,654** CITATIONS

SEE PROFILE

Mark L Paddock
University of California, San Diego
107 PUBLICATIONS **3,333** CITATIONS

SEE PROFILE

ELSEVIER

Biochimica et Biophysica Acta 1458 (2000) 148–163

BIOCHIMICA ET BIOPHYSICA ACTA
BBA

www.elsevier.com/locate/bba

Review

Proton and electron transfer in bacterial reaction centers

M.Y. Okamura *, M.L. Paddock, M.S. Graige, G. Feher

University of California, San Diego, La Jolla, CA 92093-0319, USA

Received 1 November 1999; accepted 1 December 1999

Abstract

The bacterial reaction center couples light-induced electron transfer to proton pumping across the membrane by reactions of a quinone molecule Q_B that binds two electrons and two protons at the active site. This article reviews recent experimental work on the mechanism of the proton-coupled electron transfer and the pathways for proton transfer to the Q_B site. The mechanism of the first electron transfer, $k_{AB}^{(1)}$, $Q_A^- Q_B \rightarrow Q_A Q_B^-$, was shown to be rate limited by conformational gating. The mechanism of the second electron transfer, $k_{AB}^{(2)}$, was shown to involve rapid reversible proton transfer to the semiquinone followed by rate-limiting electron transfer, $H^+ + Q_A^- Q_B^- \Leftrightarrow Q_A^- Q_B H \rightarrow Q_A (Q_B H)^-$. The pathways for transfer of the first and second protons were elucidated by high-resolution X-ray crystallography as well as kinetic studies showing changes in the rate of proton transfer due to site directed mutations and metal ion binding.

1. Introduction

Light-induced proton transport across membranes of photosynthetic bacteria results from proton-coupled electron transfer reactions in a membrane protein, the bacterial reaction center (RC) (for reviews see [1–3]). Light absorbed by the RC initiates electron transfer from a special pair of bacteriochlorophylls through a series of electron acceptors to reduce a bound ubiquinone (Q_{10}) molecule, called Q_B (see Fig. 1). The full reduction of the quinone to quinol requires the transfer of two electrons and is coupled to the uptake of two protons from solution.

$$Q_B + 2e^- + 2H^+ \Rightarrow Q_B H_2 \quad (1)$$

Following reduction, the quinol is released from the RC into the membrane and reoxidized by the cytochrome bc_1 complex, releasing protons on the opposite side of the membrane. The transport of protons across the membrane is coupled to cycling of the electron back to the RC via a cytochrome c_2 molecule. This light induced proton pump gives rise to a transmembrane proton gradient that is utilized for ATP synthesis [4,5].

The focus of research on proton transfer in bacterial RCs has been the proton-coupled electron transfer reactions of Q_B. A great deal of progress has been made using site directed mutagenesis of residues near the Q_B site. This has been the subject of several reviews [6–11]. In this review, we will focus on recent work on the mechanism of proton-coupled electron transfer reactions of Q_B and the pathway of proton transfer into the Q_B site.

2. Structure of the Reaction Center

The RC is a pigment-protein complex that can be isolated from photosynthetic membranes using deter-

* Corresponding author.

0005-2728/00/$ – see front matter
PII: S0005-2728(00)00065-7

gents. It contains three major subunits called L, M and H. The L and M subunits each contain five transmembrane α-helices and form a complex that binds the pigments and cofactors. The H subunit contains only one transmembrane α-helix. The major part of the H subunit is located on the cytoplasmic surface of the RC over the quinone-binding region. The high-resolution structures of the bacterial RCs from *Rhodopseudomonas viridis* [12] and *Rhodobacter sphaeroides* [13,14] have been obtained by X-ray diffraction. The arrangement of cofactors in the RC from *Rb. sphaeroides* is shown schematically in Fig. 1. On one side of the RC near the periplasmic surface is the bacteriochlorophyll dimer that serves as the primary electron donor (D). Two sets of cofactors involving bacteriochlorophyll, bacteriopheophytin and ubiquinone are arranged in two branches (labeled A and B) spanning the membrane. The primary electron transfer occurs predominantly along the A branch from the bacteriochlorophyll dimer, $Bchl_2$, through BChl, BPh, the primary quinone, Q_A, to the secondary quinone, Q_B. The electron transfer from Q_A to Q_B spans a distance of 15 Å (edge to edge). The two quinone molecules are linked by H-bonds through a His-Fe^{2+}-His complex.

The structure of the Q_B binding site has been the most difficult feature of the RC to establish by X-ray crystallography. This reflects the fact that the secondary ubiquinone is the substrate in the RC and consequently is loosely bound to the active site. Several different structures for Q_B by different groups have been reported. For a comparison of different structures, see Lancaster et al. [15]. Most recently Ermler et al. [13] and Stowell et al. [14] reported structures for the RC in which Q_B was weakly hydrogen bonded to a region outside the binding pocket. In addition, Stowell et al. obtained a different structure for Q_B in RCs frozen under illumination, i.e. in the charge separated state $D^+Q_B^-$ [14]. They found that Q_B^- had moved by approx. 5 Å and had undergone a 180° propeller twist (see Fig. 2). In this position, Q_B^- is hydrogen bonded to His L190 and Ser L223 and to amide protons of the peptide bonds of L224 and L225. The shift in position of Q_B in the charge separated state of the RC represents a transition from an inactive to an active site and accounts for the conformational gating mechanism discussed in Section 4.3.

Another important feature of the Q_B binding site is the presence of polar and acidic residues near Q_B

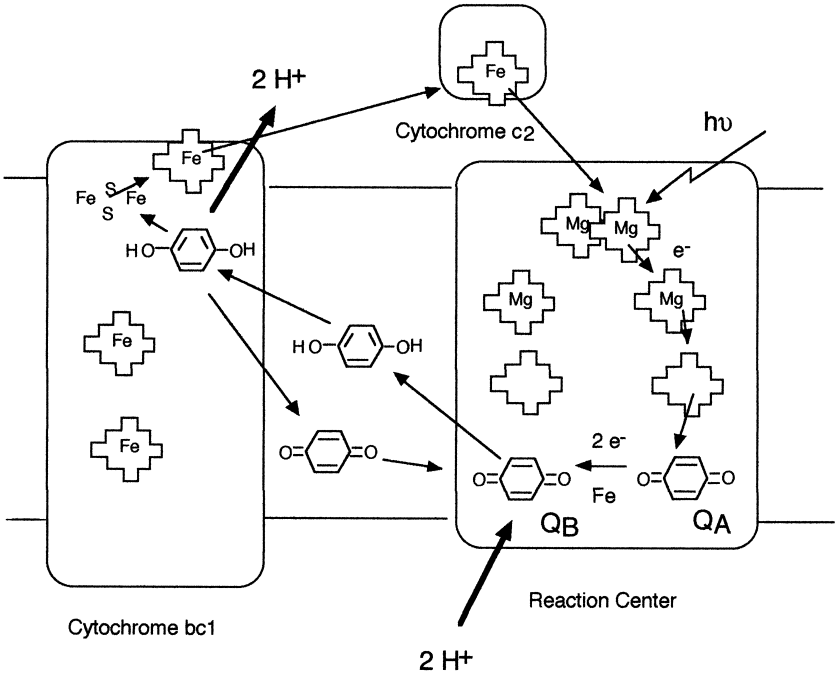

Fig. 1. Simplified representation of electron and proton transfer in photosynthetic membranes. The RC couples light-induced electron transfer to proton transfer by reducing ubiquinone at the Q_B site.

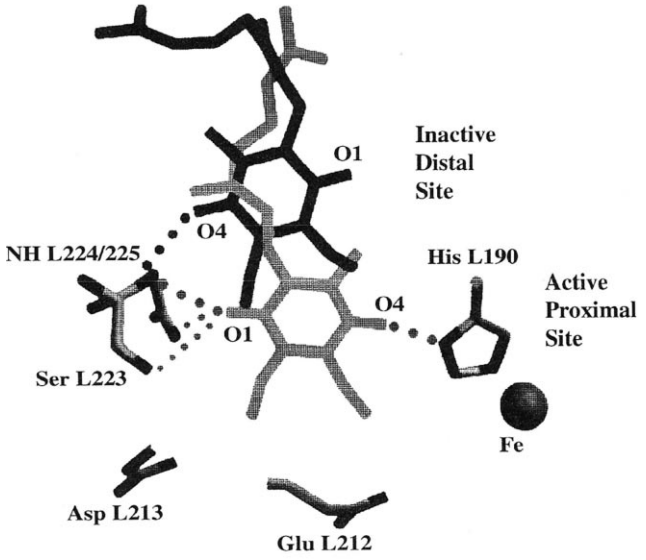

Fig. 2. Structure of the RC from *Rb. sphaeroides* showing the position of Q_B in the RC before (black) and after (gray) electron transfer [14].

that can serve as part of the pathway for proton transfer into the Q_B site. These include; Ser L223, Asp L213, Glu L212, Asp L210 as shown in Fig. 3. These residues have been studied by site directed mutagenesis (see below). In addition, recent X-ray crystal structures with improved resolution have shown chains of water molecules in the RC connecting the region near Q_B to the surface of the protein [13,14]. The longest pathway (P1) connects Q_B with the surface through a long chain of 10–12 water molecules; the P2 chain is relatively short and is connected to a pool of water molecules. P3 is a short chain through a cluster of acid residues [16]. These chains have been proposed to provide possible pathways for proton transfer [16–18] (see Fig. 3).

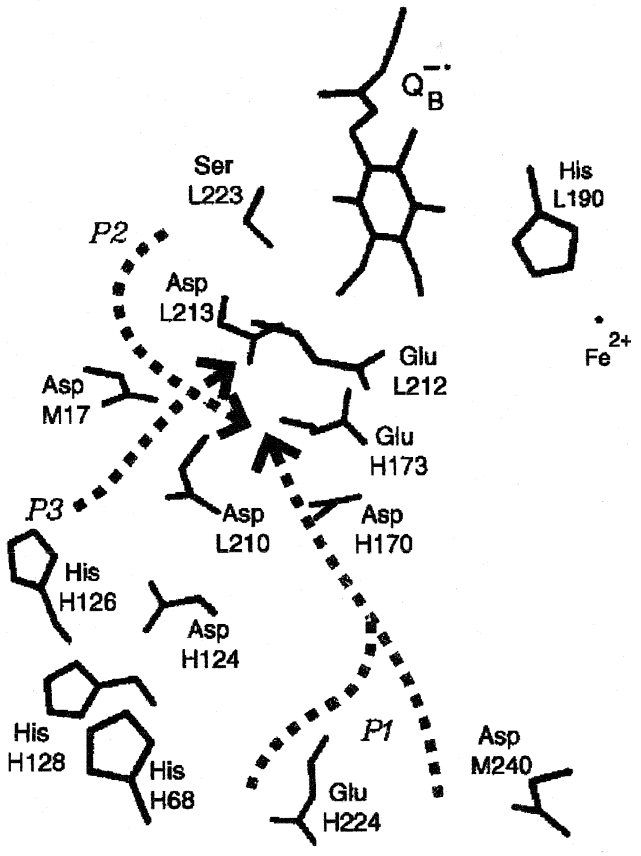

Fig. 3. Schematic representation of the Q_B site showing possible proton transfer pathways (labeled P1, P2, P3) [16]. The dominant pathway has been shown to be P3 (see Fig. 12).

3. Electron and proton transfer reactions of quinones

3.1. Quinone chemistry

Quinones are well suited for coupling electron and proton transfer reactions due to the binding of protons by quinone molecules in different redox states; quinone (Q), semiquinone (Q^-) and quinol or dihydroquinone (Q^{2-}) [4]. These states are shown in Fig. 4.

The binding of the proton by the semiquinone is relatively weak, with $pK_a \approx 5$ [19]. The binding of the two protons by the doubly reduced quinol is much stronger. Estimates of pK_a of the first and second protons in water are 14 and 12 respectively [11].

The redox potentials for ubiquinone in water have been reexamined by Wraight. He finds the midpoint potential for reduction $E_m(Q/Q^-) = -100$ to -120

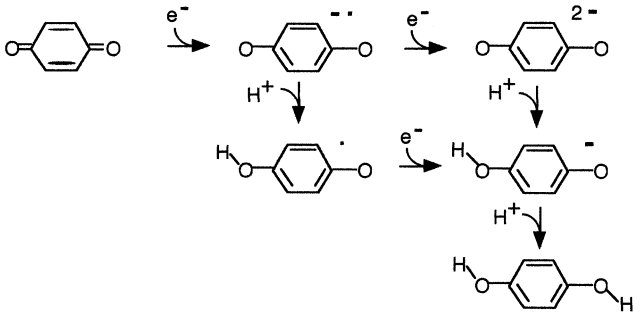

Fig. 4. Different quinone states resulting from electron and proton binding.

mV (with respect to the normal hydrogen electrode) [11]. Using this value and the average potential for the two electron reduction of +90 mV, the potential for the second electron transfer is calculated to be $E_m(Q^-/QH_2) = +280$ to +300 meV. The second electron transfer which is coupled to the binding of the two protons is more favorable (by about 400 mV) than the first. Thus, proton binding assists electron transfer, or electron transfer assists proton binding.

The properties of the quinones in the RC are modified by the protein environment to accommodate their function in the energy conversion process. The primary quinone Q_A, situated in a hydrophobic environment, accepts an electron following light induced charge separation in 200 ps and acts as the electron donor to Q_B. Q_A acts as a one electron acceptor, $E_m(Q_A/Q_A^-) = -45$ mV [20]. Further reduction of Q_A^- is normally not observed. This is probably due to the inaccessibility of Q_A to protons that are needed to stabilize the quinol state.

The secondary quinone Q_B, situated in a relatively polar environment, undergoes full reduction to the quinol in two electron reduction steps. The first and second electron reduction steps occur at the potentials, $E_m(Q_B/Q_B^-) = +20$ mV and $E_m(Q_B-/Q_BH_2) = +100$ mV [21]. These potentials are reasonably close to each other (compared to the large difference in solution of about 400 mV discussed above) and well matched to the potential of Q_A for efficient electron transfer. This matching is due to the stabilization of Q_B^- relative to Q_B, which raises the potential for the first electron reduction and lowers the potential for the second reduction [11]. The redox potentials are influenced by strong H-bonds that stabilize Q_B^- (see Fig. 2). In addition, Gunner and coworkers have emphasized (i) the role of peptide dipoles in the RC which stabilize negative charges on Q_B^- and neighboring acid groups thereby facilitating proton transfer [22] and (ii) the importance of protein flexibility in the vicinity of the Q_B site [23].

3.2. Quinone reduction cycle

The cycle of reactions in the RC involving electron and proton transfer to quinones is shown in Fig. 5.

Each step in the cycle represents a change in the state of Q_A or Q_B due to electron transfer or proton binding. The initial state DQ_AQ_B is shown at the top of the cycle. Step 1 is the photochemical reduction of Q_A, forming the state $DQ_A^-Q_B$. This step represents a combination of several electron transfer steps: the light induced electron transfer from the primary donor, through a series of intermediates, to form $D^+Q_A^-Q_B$, followed by reduction of D^+ by cytochrome c_2. Step 2 is the electron transfer from Q_A^- to Q_B with rate $k_{AB}^{(1)}$, forming the photochemically active $DQ_AQ_B^-$ state. Step 3 represents the photoinduced second electron transfer resulting in reduction of Q_A to form $DQ_A^-Q_B^-$. Step 4 is the proton-coupled second electron transfer reaction $k_{AB}^{(2)}$. The overall reaction results in the transfer of an electron and a proton to form $DQ_AQ_BH^-$. This occurs in two sequential reactions: protonation of the semiquinone Q_B^- to form the protonated intermediate semiquinone, Q_BH, followed by electron transfer (see Section 4.3). Step 5 is the binding of the second proton, giving rise to the dihydroquinone. Step 6 is the dissociation of QH_2, followed by step 7, in which a quinone is bound to form the initial state.

3.3. Electron transfer reactions

The most important reactions in the quinone reduction cycle are the two electron transfer steps in

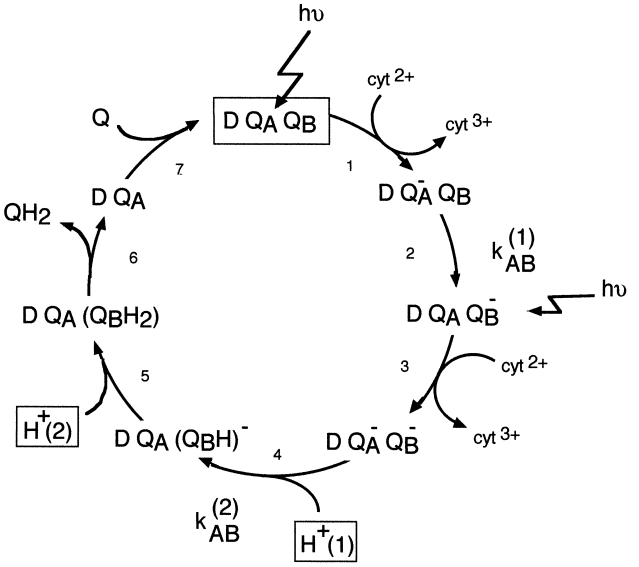

Fig. 5. The quinone reduction cycle in bacterial RCs. Q_B is reduced in two one electron reactions, $k_{AB}^{(1)}$ and $k_{AB}^{(2)}$, and binds two protons, $H^+(1)$ and $H^+(2)$. The reduced QH_2 leaves the RC and is replaced by an exogenous quinone, thereby resetting the cycle.

the reduction of Q_B. The transfer of the first electron between quinones occurs with rate $k_{AB}^{(1)}$

$$DQ_A^-Q_B \rightarrow DQ_AQ_B^- \quad k_{AB}^{(1)} \approx 10^4\ s^{-1}\ (pH\ 7) \tag{2}$$

The second electron transfer occurs with rate $k_{AB}^{(2)}$ and is coupled to uptake of the first proton

$$DQ_A^-Q_B^- + H^+(1) \rightarrow DQ_A(Q_BH)^- \quad k_{AB}^{(2)} \approx 10^3\ s^{-1}\ (pH\ 7) \tag{3}$$

Following the proton-coupled electron transfer step the second proton is rapidly bound.

$$DQ_A(Q_BH)^- + H^+(2) \rightarrow DQ_AQ_BH_2 \quad k_{H(2)} \gg 10^3\ s^{-1}\ (pH\ 7) \tag{4}$$

The second proton binding rate, $k_{H(2)}$ is generally not resolved from $k_{AB}^{(2)}$. However, the two rates can be resolved in RCs mutated to block the binding of the second proton $H^+(2)$ (see Section 5.2).

The first electron transfer step, Eq. 2 ($k_{AB}^{(1)}$), is initiated by the first of two laser pulses and occurs in about 100 μs (pH 7). In the presence of cytochrome c_2, the oxidized donor D^+ is reduced. The second saturating laser pulse initiates the second electron transfer step, Eq. 3 ($k_{AB}^{(2)}$), which occurs in about 1 ms (pH 7).

The first electron transfer step $k_{AB}^{(1)}$ which involves the transfer of an electron from Q_A^- to Q_B can be monitored by measuring either electrochromic shifts of pigment bands [24–26], changes in the semiquinone optical [27,28], or infrared spectra [29,30]. The stable product in the reaction is the anionic semiquinone Q_B^-. The protonated semiquinone is not detected down to pH 4 in isolated RCs [31]. This is consistent with the stabilization of the semiquinone state Q_B^- as discussed earlier (see Section 3.1). However, proton uptake of 0.3–0.8 protons (in the pH range 5–10) associated with the reduction of Q_B due to proton binding by nearby acid residues was measured [32,33]. The amino acid residue Glu L212 has been shown to be involved in this proton uptake by infrared spectroscopy of mutants lacking this group [34,35], proton uptake measurements [36] and electrogenicity measurements [37].

The second electron transfer step is the reduction of Q_B^- by electron transfer from Q_A^-. Since the reaction involves the disproportionation of two semiquinones to form a fully oxidized and fully reduced quinone, the reaction may be monitored by measuring the decay of the semiquinone by transient optical absorption spectroscopy [25,28]. The overall reaction for this step involves binding of two protons to form the fully reduced dihydroquinone [32,38]. The proton uptake rates for this reaction in isolated RCs have been found to be the same as the observed electron transfer rate [25,38,39]. This observation is consistent with several mechanisms for sequential electron and proton transfer where one rate (i.e. either electron or proton transfer) is much faster than the other. The mechanisms for these reactions are discussed below.

4. Mechanism of proton-coupled electron transfer

Electron transfer reactions in biological systems are often coupled to other reactions, such as proton transfer or conformational changes that have major effects on the observed rates of reaction (e.g. see Hoffman and Ratner [40]). Thus, the mechanisms of the electron transfer reactions leading to the full reduction of Q_B are of fundamental interest. In addition, understanding the mechanisms of these reactions is important for interpreting the molecular basis for the effects of mutations on the rates. For instance, since $k_{AB}^{(2)}$ involves both proton and electron transfers, the mechanism (i.e. the rate-limiting step) must be known in order to determine whether the mutation alters proton transfer or electron transfer. In this section we review a method (driving force assay) for dissecting the mechanism of a complex electron transfer reaction consisting of several steps in series [31]. The use of this assay to study $k_{AB}^{(1)}$, $k_{AB}^{(2)}$ and RC modifications that affect proton transfer will then be discussed.

4.1. Driving force assay

The mechanism of the electron transfer reactions between quinones has been elucidated using the dependence of the rate on the driving force (the driving force is equal to $-\Delta G$ for electron transfer). The assay is based on the characteristic increase in the rate of an electron transfer reaction with increasing

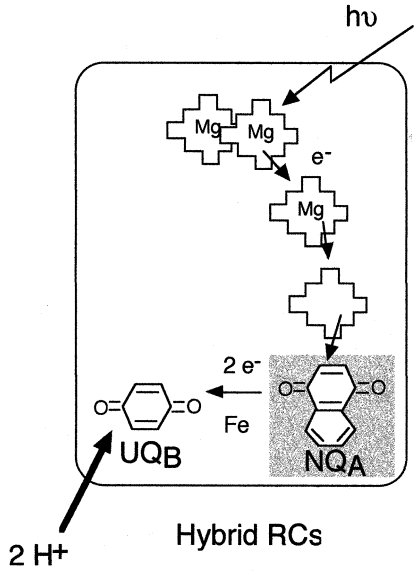

Fig. 6. Quinone substitutions in the driving force assay. Different naphthoquinone molecules, NQ_A (see shaded area), were substituted in the Q_A site to change the driving force for the electron transfer to ubiquinone UQ_B in the Q_B site.

driving force. The driving force for the reactions between Q_A and Q_B can be varied by removing the ubiquinone in the Q_A site and replacing it with a variety of naphthoquinones having different redox potentials (Fig. 6).

The recombination reactions $D^+Q_A^- \rightarrow DQ_A$ [41], and $D^+Q_AQ_B^- \rightarrow DQ_AQ_B$ [42], have been extensively studied using Q_A substitution. The rates of these reactions are sensitive to the energy of the Q_A^- state. Consequently, measurements of these rates can be used to determine the change in driving force for electron transfer from Q_A^- to Q_B.

The driving force dependence of the observed rate can be used to identify whether the rate of a complex electron transfer reaction is limited by electron transfer or some other process, e.g. proton transfer. As a simple example, consider the sequential two step reaction where the first step is a reaction to an intermediate state, $\{Q_A^-Q_B\}^*$, followed by electron transfer:

$$Q_A^-Q_B \rightarrow \{Q_A^-Q_B\}^* \rightarrow Q_AQ_B^- \quad (5)$$

The first reaction may involve a proton transfer reaction or change in protein conformation, but in either case is independent of driving force. Thus, if the first step is rate limiting, the rate will be independent of driving force. However, if the second step, i.e. electron transfer, is rate limiting, the rate will depend on driving force. Thus, from the driving force assay, one can determine which step is rate limiting without having to resolve the individual steps in the reaction. For more complex reaction mechanisms, the driving force dependence can be calculated [31].

The dependence of the electron transfer rate on the driving force can be described by the Marcus theory [43]:

$$\ln k_e = -(-\Delta G^0 - \lambda)^2/4\lambda k_B T + \text{Constant} \quad (6)$$

where λ is the reorganization energy, which for reactions of Q_B typically has a value close to 1.0 eV [42]. k_B is Boltzmann's constant, T, the temperature and ΔG^0 is the standard free energy change for the reaction. For $k_{AB}^{(1)}$ and $k_{AB}^{(2)}$ the driving force is much smaller than the reorganization energy and the rate should increase by about a factor of 10 for each 100 meV in driving force according to Eq. 6. For reactions that are not limited by the rate of electron transfer, the free energy dependence should differ from the rate predicted by the Marcus theory and can be calculated from the mechanism of the reaction [31]. Thus, the driving force assay can be used to determine the mechanism of the reaction.

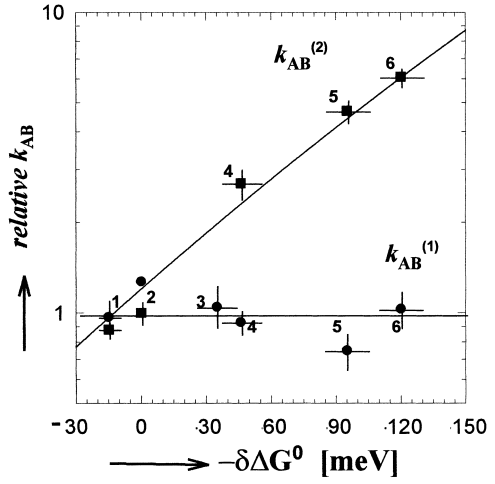

Fig. 7. Driving force dependence of $k_{AB}^{(1)}$ and $k_{AB}^{(2)}$. The driving force independence of $k_{AB}^{(1)}$ shows that electron transfer is not the rate-limiting step, indicating a conformational gating mechanism [28]. The driving force dependence of $k_{AB}^{(2)}$ is characteristic of electron transfer, indicating a proton activated electron transfer mechanism [31]. The sloping line was fitted with Eq. 6 using $\Delta G^0 = -250$ meV, $\lambda = 1.1$ eV.

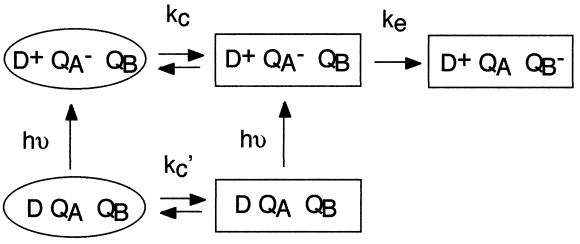

Fig. 8. The reaction sequence of the conformational gating model. The inactive (ovals) form of the RC must be converted into an active (rectangles) form before electron transfer can occur. The inactive state is stable in the dark and converts to the active state with rate k_c.

4.2. First electron transfer $k_{AB}^{(1)}$

The first electron transfer reaction was studied by Graige et al. [28] using the driving force assay. A plot of the logarithm of the relative rate $k_{AB}^{(1)}$ for the first electron transfer vs. driving force is shown in Fig. 7.

The rate is independent of driving force, in contrast to the dependence expected from the Marcus theory, showing that the rate is not limited by electron transfer. This result can be explained by a conformational gating model in which the RC can exist in two conformational states, an active and an inactive state (see Fig. 8). In the dark, the inactive state predominates. Following light absorption the electron transfer to Q_B involves two steps, a conformational step (k_c) and an electron transfer step (k_e).

In this model, the observed rate is not limited by electron transfer but is limited by the rate of the conformational gating. This mechanistic result is consistent with the observations by Stowell et al. [14] of different conformations of Q_B before and after illumination (see Fig. 2). The initial state, observed in the dark (distal position), is inactive in electron transfer (for kinetic and/or thermodynamic reasons). Movement of the quinone into the active state (proximal position) is proposed to be the rate-limiting step.

The model explains previous results of Kleinfeld et al. [44] who observed that electron transfer from Q_A^- to Q_B proceeds in RCs cooled to cryogenic temperature under illumination, but does not proceed in RCs cooled in the dark. RCs cooled in the dark are in the inactive conformation (distal state in Fig. 2). At low temperature, there is insufficient thermal energy for conformational interconversion. RCs cooled under illumination are frozen in the active proximal state and are therefore, capable of electron transfer.

The gating model predicts that fast electron transfer could be observed if a fraction of RCs have Q_B bound in the proximal position in the dark. Indeed, fast kinetics (in the μs range) have been observed in measurements of electrochromic shifts by Tiede et al. [45], and in infrared measurements by Hienerwadel et al. [29]. Li et al. have observed fast kinetics in RCs containing naphthoquinones in the Q_A site [27]. They find that the rate of reaction increases with increasing driving force, supporting the view that these represent intrinsic electron transfer processes [46].

The conformational gating model is supported by the observations of Utshig et al. [47] that $k_{AB}^{(1)}$ is decreased by Zn^{2+} binding. The binding site was proposed to be far from Q_B due to the lack of electrostatic interactions between Zn^{2+} and Q_B^-. Paddock et al. [48] confirmed this result and found that other metals (including Cd^{2+}, Ni^{2+}, and Co^{2+}) were also able to produce this effect. They also found that metal binding reduced the second electron transfer rate $k_{AB}^{(2)}$ (see below). The position of the Zn^{2+} binding site was determined by X-ray diffraction [97] to be located close to a cluster of residues His H126, His H128 and Asp H124, near the surface of the protein on the H subunit at a distance 18 Å away from Q_B (see Fig. 3). The effect of Zn^{2+} binding on $k_{AB}^{(1)}$ can be explained by a conformational gating model by postulating a change of the protein conformation or by changes in the proton transfer rate produced by metal binding [47]. An alternate mechanism in which the metal binding changes the rate of water efflux from the quinone binding site is suggested by the proximity of the metal binding site to water chains [48].

The molecular basis for the rate of the conformational gating step involves more than unhindered diffusion of the quinone into the Q_B pocket. This is indicated by the observation that the rate is independent of the length of the hydrophobic tail on Q_B [28]. The involvement of protein dynamics and/or proton transfer in $k_{AB}^{(1)}$ is supported by a number of observations. Brzezinski et al. [49] found an electrogenic transient upon Q_A^- formation in the 100 μs time scale that occurred in the absence of electron transfer to Q_B and proposed that this might repre-

sent a conformational change associated with $k_{AB}^{(1)}$. Maróti and Wraight [50] found that proton uptake upon Q_A^- formation occurs on a time scale and with an activation energy characteristic of $k_{AB}^{(1)}$, suggesting that both events might be limited by protein dynamics.

Computational studies have suggested mechanisms that might be involved in the movement of Q_B. Alexov and Gunner [23], in recent electrostatic calculations utilizing multiple configurations of protein residues, found that the rearrangement of residues near Q_B helps to stabilize the Q_B^- state. They reported that a transfer of a proton from Asp L210 to Asp L213 and the movement of Ser L223, breaking a H-bond with Asp L213 (to form a H-bond to Q_B^-), stabilize the electron on Q_B^-. This scenario was also suggested by Lancaster and Michel on the basis of the RC structure [51]. Molecular dynamics simulations by Grafton and Wheeler [52] have shown that the movement of Q_{10} into the binding pocket (proximal site) occurs rapidly for RCs in which Asp L213 and Glu L212 are protonated. They suggest that the barrier for the movement of the quinone is the protonation of these acid groups. This model can explain the decrease in $k_{AB}^{(1)}$ with increasing pH above pH 8 [72]. However at low pH, $k_{AB}^{(1)}$ is pH independent, suggesting that the rate-limiting step is controlled by some other process, e.g. conformational gating as discussed above. This is supported by the double mutant in which Asp L213 and Glu L212 are changed to neutral, non-titratable residues (Asn and Gln). In this mutant, $k_{AB}^{(1)}$ has approximately the same value as in native RCs [53].

Several dynamical processes on the 100 μs time scale initiated by Q_A reduction discussed above suggest the possibility that conformational motion may be triggered by forming Q_A^-. In such a triggered conformational gating process the electron transfer to form Q_A^- would result in a protein conformational/proton transfer event leading to the movement of Q_B into the active proximal site, followed by rapid electron transfer. This would imply that a coupling between Q_A and Q_B sites exists and that $k_c > k_c'$ (see Fig. 8). Evidence for coupling between Q_A and Q_B sites comes from (1) the effects of inhibitors bound in the Q_B site on the EPR spectrum of Q_A^- [54] and on the redox potential of Q_A [55], and (2) proton binding by Glu L212 near the Q_B site in response to Q_A reduction [36]. The functional linkage between the Q_A and Q_B sites has been proposed to involve coupling between the two quinones mediated by the His-Fe^{2+}-His complex [11,36]. The linkage may also involve electrostatic interactions between Q_A^- and Glu L212 [56,57]. In summary, the results show that the first electron transfer rate $k_{AB}^{(1)}$ is determined by conformational gating; the question of which of the possible gating steps limits the reaction remains an unresolved issue.

4.3. The second electron transfer $k_{AB}^{(2)}$

The $k_{AB}^{(2)}$ reaction (Eq. 3) involves the transfer of the second electron to Q_B^- as well as the binding of the first proton, $H^+(1)$. The question of whether the first proton transfer precedes or follows electron transfer, and which of these is the rate-limiting step was investigated using the driving force assay [31]. Four possible cases involving two sequential steps were considered: the mechanisms in which proton transfer precedes electron transfer, or in which electron transfer precedes proton transfer (the upper and lower sequences of reactions shown in Fig. 9). In addition, a mechanism in which proton transfer and electron transfer occurred in a concerted fashion [58] (Fig. 9, horizontal arrow) was also considered. Each reaction step in each sequence could be the rate-limiting step, giving rise to five possible cases shown in Fig. 9.

The dependence of the overall rate on the driving force is different for each of the cases. The dependence of $k_{AB}^{(2)}$ on driving force was measured and

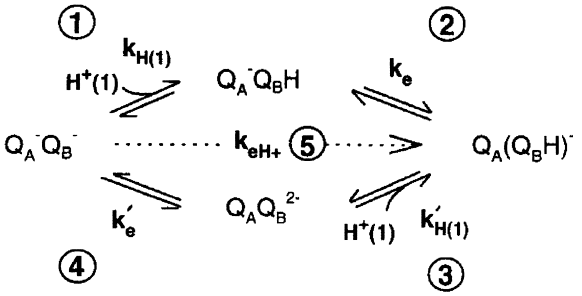

Fig. 9. Possible mechanisms for the proton-coupled electron transfer, $k_{AB}^{(2)}$. Five different cases result when different reaction steps are rate limiting. The circled numbers, 1–4, denote the rate-limiting steps in a two-step mechanism. The dashed line, 5, represents a concerted mechanism.

compared to predictions for the different cases [31]. The result shows a characteristic Marcus-like driving force dependence, indicating that electron transfer is the rate-limiting step (see Fig. 7). The cases where electron transfer is the rate-limiting step and follows proton transfer, i.e. step 2 in Fig. 9, gave the best fit to the data. The case where electron transfer occurred before proton transfer, i.e. where step 4 in Fig. 9, was rate limiting, had a slightly steeper slope, due to the smaller, i.e. negative, driving force. This case could be ruled out by a study in which the driving force was changed by mutations altering the electrostatic interaction in the Q_B site [59]. The concerted mechanism was ruled out by a study in which the protonated semiquinone intermediate state was observed using a quinone with a higher pK_a [60]. The results show that fast reversible proton transfer to the semiquinone followed by rate-limiting electron transfer is the dominant mechanism in $k_{AB}^{(2)}$.

In the proton activated electron transfer (PAET) mechanism for $k_{AB}^{(2)}$, described above, the reaction goes through a protonated semiquinone intermediate, $Q_A^- Q_B H$ (see Fig. 10). Although this state is sparsely populated relative to the anionic semiquinone state, because of the unfavorable proton binding energy, ΔG_H^0, it dominates the electron transfer reaction due to the increased driving force ΔG_e^0 (see Fig. 10) and the lower probability of forming the Q_B^{2-} state. The rate of reaction is proportional to the product of the fraction of the semiquinone in the protonated state, f($Q_B H$) and the intrinsic electron transfer rate, k_e, to the protonated semiquinone, $Q_B H$:

$$k_{AB}^{(2)} = f(Q_B H) k_e \quad (7)$$

The PAET mechanism shown in Fig. 10 was verified by the observation of the protonated semiquinone state using rhodoquinone in the Q_B site (rhodoquinone is a ubiquinone with an amine substituted for a methoxy group, leading to a higher pK_a) [60]. The rhodoquinone substitution allowed the measurement of the intrinsic k_e since for $pH < pK_a$, $f(Q_B H) = 1$. Based on the rhodoquinone results, the values for $f(Q_B H)$ and k_e in native RCs (containing ubiquinone) were calculated. The results are that at pH 7.5 the intrinsic electron transfer rate $k_e \approx 10^6$ s^{-1} and the fraction of protonated semiquinone, $f(Q_B H) \approx 10^{-3}$.

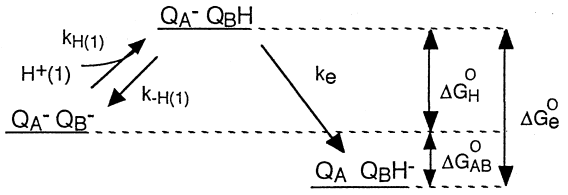

Fig. 10. Energy level scheme for proton activated electron transfer. For native RCs the estimated values (at pH 7.5) are: $\Delta G_{AB}^0 = -70$ meV, $\Delta G_H^0 = 180$ meV, $\Delta G_e^0 = -250$ meV [60].

Since proton transfer is not the rate-limiting step in native RCs, the proton transfer rate constant $k_{H(1)}$ (see Fig. 10) cannot be directly determined. However, since the proton transfer rate must be faster than the observed $k_{AB}^{(2)}$, an estimate of the lower limit of $k_{H(1)} \geq 10^3$ s^{-1} is obtained. A faster limit for $k_{H(1)} \geq 10^4$ s^{-1} is obtained using RCs containing NQ in the Q_A site to increase k_e [60]. An additional constraint in the mechanism is that the rate of dissociation from the protonated semiquinone $k_{-H(1)}$ (see Fig. 10) must be faster than the intrinsic electron transfer rate. Since the intrinsic rate has been estimated to be $k_e \approx 10^6$ s^{-1}, the dissociation rate $k_{-H(1)} \geq 10^6$ s^{-1}.

Although the driving force assay shows that in native RCs the proton transfer rate cannot be obtained from the measured $k_{AB}^{(2)}$, it provides a means for testing whether a mutation makes proton transfer the rate-limiting step. Thus, the driving force assay provides a useful method for studying the effects of mutations on the rate of proton transfer. This is discussed in the next section.

5. Pathways for proton transfer

The location of the Q_B site in the interior of the RC presents a problem for the transport of a proton from the aqueous exterior through the low protein dielectric. The solution to this problem is a pathway for proton transfer through which protons can be readily conducted. One factor in such a pathway is the presence of a chain of proton donor and acceptor groups linked by hydrogen bonds (or at least within hydrogen bonding distance) [61]. The donor and acceptor groups can include protonatable amino acid residues such as Asp, Glu, Ser, Thr, His, Lys and Arg or internal chains of hydrogen-bonded water

molecules. The rate of proton transfer through such a chain of proton donor and acceptor groups depends on the positioning of the hydrogen-bonded groups (over distances of 3–4 Å). A second important factor is favorable energetics for proton binding, determined by the pK_a of each group and the internal electrostatic potential [96]. The pathway for proton transfer to the Q_B site has been studied by a variety of methods. These include structural, mutational, and more recently, metal binding studies.

5.1. Pathway of first proton, $H^+(1)$

The pathway for proton transfer was studied by mutation of protonatable residues near the Q_B site. The first proton $H^+(1)$, according to the PAET mechanism, is bound prior to the second electron transfer step (Fig. 5). Thus, the mutation of residues in the pathway for $H^+(1)$ should block the proton activated second electron transfer reaction $k_{AB}^{(2)}$. Two residues, Asp L213 and Ser L223, located at the outer edge of the Q_B binding pocket (see Fig. 2), had large effects on $k_{AB}^{(2)}$ when mutated to non-protonatable residues. Reductions of $k_{AB}^{(2)}$ by 3000 and 300 were observed in DN(L213) RCs [62–64] and SA(L223) RC, respectively [65–67] (see Table 1).

The Asp L213 mutation to Asn made $k_{AB}^{(2)}$ independent of driving force [68] (see Fig. 11) showing that the proton transfer rate was reduced and now was the rate-limiting step. This is strong evidence for the involvement of Asp L213 in the pathway for proton transfer.

The Ser L223 mutation, despite its large effect on $k_{AB}^{(2)}$, did not make the reaction independent of driving force (see Fig. 11). The lower value for $k_{AB}^{(2)}$ in this mutant can be accounted for by the lower fraction of protonated semiquinone (see Eq. 7). The smaller effect of the mutation, Ser L223→Ala, compared to the Asp L213→Asn mutation, can be explained by alternate pathways for proton transfer, e.g. by direct proton transfer from Asp L213 to Q_B^-, or by a mechanism in which a bridging water molecule replaces Ser L223. The involvement of a bridging water molecule was tested by constructing the mutation Ser L223→Gly, in which the smaller Gly residue should allow space for an internal water molecule. In this mutant $k_{AB}^{(2)}$ is not decreased, consistent with the presence of a bridging water molecule in the position of the Ser OH group [69]. These results support a proton transfer role for the hydroxyl group from Ser L223 to Q_B^-.

Mutational studies of acid residues located further from the Q_B site had smaller effects on $k_{AB}^{(2)}$. These mutations included: Asp L210→Asn [70], Asp M17→Asn [98] and Glu H173-Gln [71]. These mutations affected $k_{AB}^{(1)}$ and $k_{AB}^{(2)}$ only by factors of 2–10. Baciou and Michel [17] made mutations of Pro L209 to Phen and Tyr with the aim of disrupting the P1 water chain (see Fig. 3) proposed to be involved in the proton transfer pathway. The Tyr and Phe mu-

Table 1
Relative reduction in rates of electron transfer $k_{AB}^{(1)}$ and $k_{AB}^{(2)}$ in modified RCs of *Rb. sphaeroides* (pH 7.5)

Name	Notation	$k_{AB}^{(1)}$ native/$k_{AB}^{(1)}$ mutant	$k_{AB}^{(2)}$ native/$k_{AB}^{(2)}$ mutant	Rate-limiting step[a]	Ref.
Native	–	1.0	1.0	e^-	
Asp L213→Asn	DN(L213)	17	6000	H^+	[61–63]
Ser L223→Ala	SA(L223)	0.4	400	e^-	[64–66]
Glu L212→Gln	EQ(L212)	1.3	1.4	e^-	[72–74]
Asp L210→Asn	DN(L210)	7	2.4	e^-	[69]
Asp M17→Asn	DN(M17)	8	2.0	e^-	[b]
Glu H173→Gln	EQ(H173)	4	8.1	e^-	[70,71]
Pro L209→Phe	PF(L209)	7	15	n.d.	[17]
RC+Cd^{2+}	–	10	20	H^+	[47]
Asp L213→Asn/Asn-M44→Asp	DN(L213)/ND(M44)	1.3	1.0	e^-	[67]
Asp L213→Asn/Arg-M233→Cys	DN(L213)/RC(M233)	1.4	12.0	e^-	[67]

[a]Rate-limiting step, either electron transfer (e^-) or proton transfer (H^+), determined using the driving force assay.
[b]M. Paddock, unpublished.

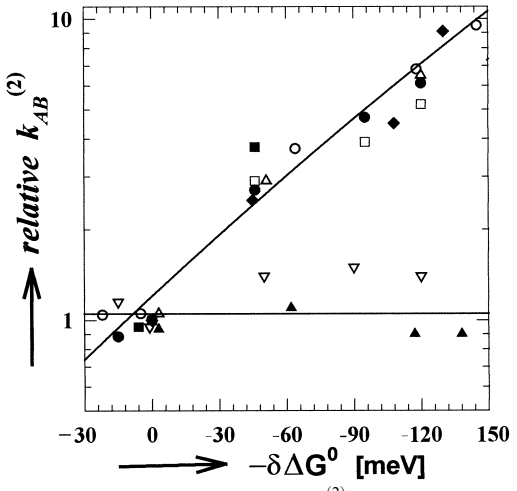

Fig. 11. Driving force dependence of $k_{AB}^{(2)}$ in modified RCs. The driving force dependence characteristic of rate-limiting electron transfer was found for native RCs (●) and in most mutant RCs: ○, SA(L223); ■, ED(L212); □, DN(L210); △, DE(L213); ◆, EQ(L212). The driving force independence characteristic of rate-limiting proton transfer was found for DN(L213) RCs (▲) and RCs in which Cd^{2+} was bound (▽). Modified from [31,48,68].

tations resulted in reductions of $k_{AB}^{(2)}$ by factors of 4 and 15 (pH 7.5) that was proposed as evidence supporting the involvement of the P1 pathway in proton transfer. Although these mutations affect $k_{AB}^{(2)}$, these effects are by themselves not conclusive evidence for the involvement of these residues in the proton transfer pathway, since $k_{AB}^{(2)}$ depends on the fraction of protonated semiquinone and the rate of electron transfer (see Eq. 7). The fraction can be changed by interactions that alter the stability of Q_BH. This would change the pK_a of the semiquinone and thus change $k_{AB}^{(2)}$. In addition mutations can change the electron transfer rate k_e and thus produce a change in $k_{AB}^{(2)}$. Thus a change in $k_{AB}^{(2)}$ can be obtained without altering the rate of proton transfer through the pathway. In order to conclude that changes in $k_{AB}^{(2)}$ are due to proton transfer, further evidence that proton transfer is modified need to be obtained.

The pathway for proton transfer has been elucidated by recent studies of the effect of metal binding on $k_{AB}^{(2)}$. Paddock et al. [48] showed that stoichiometric binding of the divalent metal ions, Cd^{2+}, Zn^{2+} to the RC reduces the measured $k_{AB}^{(2)}$ by factors of 20 and 10, respectively. In addition, $k_{AB}^{(2)}$ in metal inhibited RCs was independent of driving force (see Fig. 11). Thus, the metal binding reduced the proton transfer rate by at least a factor of 10^2 making it the rate-limiting step. RCs with mutations at Asp L210 and Asp M17 exhibited 10-fold larger decreases in $k_{AB}^{(2)}$ due to metal binding than native RCs showing that these residues are involved in the proton transfer pathway [98].

The location of the metal binding site was determined by X-ray diffraction studies (H. Axelrod et al., unpublished). The Cd^{2+} and Zn^{2+} were found to bind to His H126, His H128 and Asp H124 near the surface of the RC close to the P3 pathway (see Fig. 3). Simultaneous replacement of His H126 and His H128 with Ala reduced the binding of metals by more than two orders of magnitude showing that in solution the binding site involves His H126 and His H128 as observed in crystals of native RCs [99]. The close proximity of the metal binding site to the proton transfer pathway strongly suggests that the metal binding blocks proton transfer at or near the P3 pathway. The blockage may occur because one of the ligands (e.g. His H126 or His H128) has been eliminated as the initial proton donor or because of electrostatic or steric restrictions to proton transfer. An alternate explanation is that the metal binding produces protein conformational changes that modify the structure and dynamics at distant sites, in analogy to a proposed explanation of the metal effects on $k_{AB}^{(1)}$ [47] (see Section 4.1). An argument against this explanation is that no long-range changes in the X-ray crystal structure are observed in RCs due to metal binding (Axelrod et al., unpublished). The slow proton transfer in metal bound RCs suggests that the proton transfer rates through alternate paths, e.g. P1 or P2, are several orders of magnitude slower than the rate through the P3 path. This shows that one pathway dominates proton transfer to Q_B^-.

5.2. Pathway of second proton $H^+(2)$

The second proton bound by Q_B is taken up after the second electron transfer step (see Fig. 5). The basis for this assignment is the observation that in RCs containing the mutation of Glu L212 → Gln, the transfer of the first proton and the second electron transfer rate are unchanged (see Table 1), but the transfer of the second proton is blocked [72–74]. The unchanged $k_{AB}^{(2)}$ indicates that the second proton

is not required for electron transfer. The blockage of the second proton due to the mutation of Glu L212 could be monitored by the inhibition of the turnover of the RC after uptake of three electrons, i.e. at the state $Q_A^-(Q_BH)^-$ [72,73], or by monitoring the blockage of electron transfer to the cytochrome *bc*1 complex in membranes, i.e. inhibition of quinol release by the mutation [74]. These results implicate Glu L212 as an important residue for transfer of the second proton (see Fig. 12).

The pathway of proton transfer from Glu L212 to Q_BH^- is not clear from the static structures of the RC. Glu L212 is located in the interior edge of the Q_B binding pocket, close to the Fe liganded His L190 that provides a hydrogen bond to the bound Q_B. However, Glu L212 is not hydrogen bonded to the terminal proton acceptor (the carbonyl oxygen O4 bound to His 190). Thus, the movement of the doubly reduced quinol may be required to bring Glu L212 in close contact with O4 as it moves out of the Q_B site. The proton transfer pathway to Glu L212 from the surface seems most likely to have the same entry point as that of $H^+(1)$. Since the protonation of Glu L212 from solution occurs in the first electron transfer step, $k_{AB}^{(1)}$, as shown by infrared [34,35], and proton uptake measurements [36,37], the finding that metal binding affects $k_{AB}^{(1)}$ in native RCs but not in EQ L212 RCs lacking Glu L212 (P. Ädelroth, unpublished) shows that the uptake of $H^+(2)$ is blocked by metal binding. This indicates that the entry point for $H^+(2)$ is the same as for $H^+(1)$.

The proposed pathways for $H^+(1)$ and $H^+(2)$ based on mutation and metal-binding arguments are shown in Fig. 12. The pathway for $H^+(1)$ starts near His H126, His H128 and proceeds through the regions near Asp M17 and Asp L210 to Asp L213, Ser L223 and finally to Q_B^-. The detailed trajectory of the proton near the surface is not certain but may involve several parallel paths in the region near Asp M17 and Asp L210 that explains why mutations of either of these groups have smaller effects than mutations of Asp L213 (see Table 1). The pathway for $H^+(2)$ terminates at Glu L212 and most likely follows the same initial path as $H^+(1)$. The characteristic feature of the protein in the region of these pathways is a cluster of negatively charged acid residues that stabilize the proton in the interior of the protein, and water molecules that connect protonatable groups. The large number of acid groups and water molecules in the pathway probably contribute to the fast rate of proton transfer.

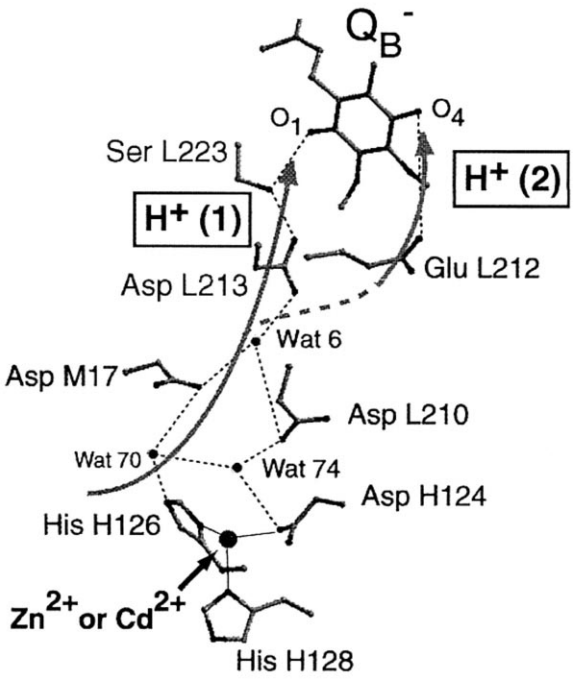

Fig. 12. Proposed pathways for proton transfer (dashed lines) to Q_B in RCs from *Rb. sphaeroides*. Binding of Zn^{2+} or Cd^{2+} at the position labeled by the arrow, blocks proton transfer to Q_B^- [48].

5.3. Pathways in other species and in revertant RCs

The pathways for proton transfer discussed above and shown in Fig. 12 apply to RCs from *Rb. sphaeroides*. In RCs from *Rps. viridis* the pathways must be different since several residues of the pathway are not conserved [75]. RCs from *Rps. viridis* lack an acid residue corresponding to Asp L213. Instead of Asp L213, RCs from *Rps. viridis* have an Asp residue at position M43 (M44 in *Rb. sphaeroides*) that is believed to act in its place. This functional equivalence was shown by experiments in which RCs from *Rb. sphaeroides* were mutated to replace Asp L213 by Asn and Asn M44 by Asp. In this double mutant DN(L213)/ND(M44), RCs were found to be fully functional in proton transfer [76]. Similar conclusions were derived from experiments using second site mutation in RCs from *Rhodobacter capsulatus*.

A second site mutation of Asn M43→Asp was found to compensate for the deleterious effects of an initial mutation of Asp L213→Ala [77]. Furthermore, in RCs from *Rps. viridis*, the residues His H126 and His H128 are not conserved. However, it is interesting that in RCs from *Rps. viridis*, there are two His residues close to Asp M43 that are not present in RCs from *Rb. sphaeroides* that could perform the analogous functions. These studies show that proton transfer pathways are different in RCs from different bacterial strains.

The possibility of alternate proton transfer pathways has been emphasized by studies of second site mutations. In an extensive series of experiments, Hanson and coworkers showed that a wide variety of second site mutations in RCs from *Rb. capsulatus* were able to compensate for the deleterious mutations of the proton transfer residues, Asp L213→Ala and Glu L212→Ala [36,77–86], including the mutations Asn M43→Asp [82], Arg M231→Leu [84], Gly L225→Asp [83]. In *Rb. sphaeroides*, the mutation of Asp L213→Asn can be compensated for by Asn M44→Asp [76], Arg M233→Cys [87] and Arg H177→His [68]. An almost universal feature of these second site mutations is that the second mutation introduced a negative charge or removed a positive charge in RC. These results indicate that electrostatic interactions play an important role in proton transfer, because the negative charges stabilize protons in the interior of the protein.

A second feature of several of the second site mutations is that they need not be close to the site of the initial mutation. For instance, the second site mutation Arg M233 in *Rb. sphaeroides* and the homologous Arg M231 in *Rb. capsulatus* is approx. 13 Å away from the initial mutated residue Asp L213 and approx. 17 Å away from Q_B. In RCs from *Rb. sphaeroides*, the initial mutation has a $k_{AB}^{(2)}$ of 0.4 s^{-1} that is limited by proton transfer (see Fig. 11). The second site reverent has a $k_{AB}^{(2)}$ of 100 s^{-1} and is no longer limited by proton transfer as shown by the driving force assay (see Fig. 11) [68]. Thus, the proton transfer rate is increased at least 10^2-fold by the suppressor mutation. The structural changes associated with the change in rate have been studied by X-ray diffraction [88]. The crystal structure of the reverent RC (Asp L213→Asn/Arg M233→Cys) in *Rb. sphaeroides* shows large changes in the position of charged residues near the location of the suppressor mutation far from the Q_B site. For instance Arg H177 moves into the cavity created by the mutation and the acid residue Glu H122, which forms an ion pair with Arg M233 in native RCs, moves away. This large-scale movement (electrostatic dominos) of charged residues was proposed by Sebban et al. [84] to explain the long range propagation of the effect of mutation. In addition to these large-scale movements of charged residues, relatively small movements of neutral residues propagate into the region near Q_B. The structure of the suppressor mutant showed a water molecule with an additional H-bond to Thr L226 in the Q_B binding site that was absent in the native structure. The H-bond increases the energy required to displace this water molecule and thus could change the position of the reduced Q_B^- in the binding site. This change in structure can explain the observed decreased stability of the Q_B^- state in these mutant RCs, which is reflected in the recombination kinetics [68], as well as changes that have been observed in the infrared spectrum [89] and the EPR spectrum (M.L. Paddock, unpublished). These structural changes may be responsible for providing new pathways for proton transfer to Q_B^-. The results from the suppressor mutant emphasize the importance of small structural changes in protein structure that propagates along large distances in producing orders of magnitude changes in the rate of proton transfer.

6. Dynamics and energetics of proton transfer

A detailed description of proton transfer in the RC should include not only the path of the protons through the protein but also the energies and dynamics of the intermediate states involved. At present the details of these topics are not well understood. They remain a challenge for future research. However, studies using computational methods, infrared spectroscopy and site directed mutagenesis have shed some light on these questions.

An important feature of the region near the Q_B site is the cluster of nearby acid residues. These include Glu L212, Asp L213, Asp L210, Glu H173, Asp M17. These residues can serve to establish a negative electrostatic potential to stabilize the proton

near Q_B and also to act as proton donor/acceptor groups. The protonation of these residues has been studied by electrostatic calculations [23,56,57,90,91]. We shall discuss the general features of these calculations. For a more detailed discussion, see the article by Gunner in this issue.

Electrostatic calculations have emphasized the importance of loss of solvation energy, due to burying charged groups in the protein interior, and the importance of electrostatic interactions among charged groups in the region of the Q_B site in determining the protonation states of acid residues. The interactions within the acid cluster result in the binding of one or more protons that are shared within the acid cluster when Q_B is in the neutral oxidized state at pH 7. Calculations show that one proton is shared between Asp L213 and Glu L212, with Q_B in the neutral state, although the extent of protonation differs among the different studies (see Alexov and Gunner for a useful comparison [23]). Upon Q_B^- formation, calculations show that both residues, Glu L212 and Asp L213, become fully protonated due to the electrostatic interaction with Q_B^-. Part of the proton population required to protonate these two groups comes from solution and part from internal protonated groups within the cluster.

Infrared spectroscopy provides a useful method to monitor the proton uptake by specific groups in the RC since carboxylic acid residues display a characteristic absorption change upon protonation. In RCs from *Rb. sphaeroides* a major absorption change at 1728 cm^{-1} was observed upon Q_B^- formation and assigned to the protonation of Glu L212 [34,35], as predicted by some electrostatic calculations [56,90], but not by others [23]. However, no spectral changes due to protonation of Asp L213 could be identified. In RCs from *Rps. viridis* no carboxyl group absorption changes were identified upon Q_B^- formation [92]. Possible reasons for the differences between theory and experiment may be that the theoretical treatment of the protein dielectric is not adequate or that the infrared bands of carboxylic acids may be broadened and thereby unresolved in the experiments.

An interesting possibility that has been proposed to explain the absence of additional carboxyl bands in the infrared region is proton uptake by a highly polarizable hydrogen bond network. Such networks were first proposed by Zundel [93] to explain characteristic broad bands in the infrared spectrum in the hydrogen stretch region seen in many chemical systems. Evidence for such networks has been found in the proton pumping protein bacteriorhodopsin [94]. Breton and Nabedryk [95] have observed characteristic broad bands in the FTIR spectra of RCs upon Q_A^- and Q_B^- formation and have suggested that protons bound in a hydrogen bond network may play a role in proton transfer in RCs.

7. Conclusions

- The reduction of Q_B in bacterial RCs occurs in two one-electron reactions.
- In the first electron transfer reaction, $k_{AB}^{(1)}$, the anionic semiquinone Q_B^- is formed. The rate of this reaction is determined by a conformational gating step. No protons are taken up by the quinone, but proton binding to the internal acid group Glu L212 occurs.
- In the second electron transfer reaction, $k_{AB}^{(2)}$, rapid transient protonation of the semiquinone precedes the rate-limiting second electron transfer step. This is followed by the binding of the second proton.
- The pathway for the first proton transfer, deduced from mutational and metal binding effects, originates from a region in the protein near the H subunit residues Asp H124, His H126, His H128, and proceeds through a region near Asp M17 and Asp L210, then Asp L213 and Ser L223 to Q_B^-. The pathway for the second proton transfer involves Glu L212.
- The intrinsic rates of proton transfer $>10^4$ s^{-1} and electron transfer $>10^6$ s^{-1} are much faster than the observed overall rates of reaction which are in the range of 10^3–10^4 s^{-1}. The energetics and dynamics of the system are designed to allow favorable reaction rates with relatively small net changes in free energy.

Acknowledgements

We thank Herb Axelrod and Ed Abresch for their assistance with the crystallography, Pia Ädelroth for allowing us to quote her unpublished work and Marilyn Gunner, Thomas Beatty, Hemi Gutman,

David Silverman, Eliane Nabedryk and Jacques Breton for discussions on proton transfer. This work was supported by grants from the National Institutes of Health, GM41637 and GM 13191 and the National Science Foundation, MCB 94-16652.

References

[1] G. Feher, J.P. Allen, M.Y. Okamura, D.C. Rees, Nature 339 (1989) 111–116.
[2] M.R. Gunner, Curr. Top. Bioenerg. 16 (1991) 319–367.
[3] J. Deisenhofer, J.R. Norris, The Photosynthetic Reaction Center, vols. I and II, Academic Press, San Diego, CA, 1993.
[4] A.R. Crofts, C.A. Wraight, Biochim. Biophys. Acta 726 (1983) 149–185.
[5] W.A. Cramer, D.B. Knaff, Energy Transduction in Biological Membranes, Springer-Verlag, New York, 1990.
[6] E. Takahashi, P. Maróti, C.A. Wraight, in: E. Diemann, W. Junge, A. Muller, H. Ratajczak (Eds.), Electron and Proton Transfer in Chemistry and Biology, Elsevier Publ., Amsterdam, 1991, pp. 219–236.
[7] M.Y. Okamura, G. Feher, Annu. Rev. Biochem. 61 (1992) 861–896.
[8] V.P. Shinkarev, C.A. Wraight, in: J. Deisenhofer, J.R. Norris (Eds.), The Photosynthetic Reaction Center, Academic Press, San Diego, CA, 1993, pp. 193–255.
[9] P. Sebban, P. Maróti, D.K. Hanson, Biochimie 77 (1995) 677–694.
[10] M.Y. Okamura, G. Feher, in: R.E. Blankenship, M.T. Madigan, C.E. Bauer (Eds.), Advances in Photosynthesis: Anoxygenic Photosynthetic Bacteria, Kluwer Academic Publishers, Dordrecht, 1995, pp. 577–594.
[11] C. Wraight, in: G. Garab (Ed.), Photosynthesis: Mechanisms and Effects, Kluwer Academic Publishers, Dordrecht, 1998, pp. 693–698.
[12] J. Deisenhofer, H. Michel, EMBO J. 8 (1989) 2149–2170.
[13] U. Ermler, G. Fritsch, S.K. Buchanan, H. Michel, Structure 2 (1994) 925–936.
[14] M.H.B. Stowell, T.M. McPhillips, D.C. Rees, S.M. Soltis, E. Abresch, G. Feher, Science 276 (1997) 812–816.
[15] C.R.O. Lancaster, U. Ermler, H. Michel, in: R.E. Blankenship, M.T. Madigan, C.E. Bauer (Eds.), Advances in Photosynthesis: Anoxygenic Photosynthetic Bacteria, Kluwer Academic Publishers, Dordrecht, 1995, pp. 503–526.
[16] E.C. Abresch, M.L. Paddock, M.H.B. Stowell, T.M. McPhillips, H.L. Axelrod, S.M. Soltis, D.C. Rees, M.Y. Okamura, G. Feher, Photosynth. Res. 55 (1998) 119–125.
[17] L. Baciou, H. Michel, Biochemistry 34 (1995) 7967–7972.
[18] G. Fritzsch, L. Kampmann, G. Kapaun, H. Michel, in: G. Garab (Ed.), Photosynthesis: Mechanisms and Effects, Kluwer Academic Publishers, Dordrecht, 1998, pp. 861–864.
[19] A.J. Swallow, in: B.L. Trumpower (Ed.), Function of Quinones in Energy Conserving Systems, Academic Press, New York, 1982, pp. 59–72.
[20] P.L. Dutton, J.S. Leigh, C.A. Wraight, FEBS Lett. 36 (1973) 169–173.
[21] A.W. Rutherford, M.C.W. Evans, FEBS Lett. 110 (1980) 257–261.
[22] M.R. Gunner, A. Nicholls, B. Honig, J. Phys. Chem. 100 (1996) 4277–4291.
[23] E.G. Alexov, M.R. Gunner, Biochemistry 38 (1999) 8253–8270.
[24] A. Vermeglio, R.K. Clayton, Biochim. Biophys. Acta 461 (1977) 159–165.
[25] C.A. Wraight, Biochim. Biophys. Acta 548 (1979) 309–327.
[26] D. Kleinfeld, M.Y. Okamura, G. Feher, Biochim. Biophys. Acta 766 (1984) 126–140.
[27] J. Li, D. Gilroy, D.M. Tiede, M.R. Gunner, Biochemistry 37 (1998) 2818–2829.
[28] M.S. Graige, G. Feher, M.Y. Okamura, Proc. Natl. Acac. Sci. USA 95 (1998) 11679–11684.
[29] R. Hienerwadel, D. Thibodeau, F. Lenz, E. Nabedryk, J. Breton, W. Kreutz, W. Mäntele, Biochemistry 31 (1992) 5799–5808.
[30] R. Brudler, K. Gerwert, Photosynth. Res. 55 (1998) 261–266.
[31] M.S. Graige, M.L. Paddock, J.M. Bruce, G. Feher, M.Y. Okamura, J. Am. Chem. Soc. 118 (1996) 9005–9016.
[32] P. Maróti, C.A. Wraight, Biochim. Biophys. Acta 934 (1988) 329–347.
[33] P.H. Mcpherson, M.Y. Okamura, G. Feher, Biochim. Biophys. Acta 934 (1988) 348–368.
[34] R. Hienerwadel, S. Grzybek, C. Fogel, W. Kreutz, M.Y. Okamura, M.L. Paddock, J. Breton, E. Nabedryk, W. Mäntele, Biochemistry 34 (1995) 2832–2843.
[35] E. Nabedryk, J. Breton, R. Hienerwadel, C. Fogel, W. Mantele, M.L. Paddock, M.Y. Okamura, Biochemistry 34 (1995) 14722–14732.
[36] J. Miksovska, P. Maróti, J. Tandori, M. Schiffer, D.K. Hanson, P. Sebban, Biochemistry 35 (1996) 15411–15417.
[37] P. Brzezinski, M.L. Paddock, M.Y. Okamura, G. Feher, Biochim. Biophys. Acta 1321 (1997) 149–156.
[38] P.H. McPherson, M.Y. Okamura, G. Feher, Biochim. Biophys. Acta 1144 (1993) 309–324.
[39] P. Maróti, C.A. Wraight, in: M. Baltscheffsky (Ed.), Current Research in Photosynthesis, Kluwer, Dortrecht, 1990, pp. 1.165–1.168.
[40] B.M. Hoffman, M.A. Ratner, J. Am. Chem. Soc. 109 (1987) 6237–6243.
[41] N.W. Woodbury, W.W. Parson, M.R. Gunner, R.C. Prince, P.L. Dutton, Biochim. Biophys. Acta 851 (1986) 6–22.
[42] A. Labahn, J. Bruce, M. Okamura, G. Feher, J. Chem. Phys. 197 (1995) 355–366.
[43] R.A. Marcus, N. Sutin, Biochim. Biophys. Acta 811 (1985) 265–322.
[44] D. Kleinfeld, M.Y. Okamura, G. Feher, Biochemistry 23 (1984) 5780–5786.
[45] D.M. Tiede, J. Vázquez, J. Córdova, P.A. Marone, Biochemistry 35 (1996) 10763–10775.

[46] J. Li, M. Gunner, Biophys. J. 76 (1999) A240.
[47] L.M. Utschig, Y. Ohigashi, M.C. Thurnauer, D.M. Tiede, Biochemistry 37 (1998) 8278–8281.
[48] M.L. Paddock, M.S. Graige, G. Feher, M.Y. Okamura, Proc. Natl. Acad. Sci. USA 96 (1999) 6183–6188.
[49] P. Brzezinski, M.Y. Okamura, G. Feher, in: J. Breton, A. Vermeglio (Eds.), The Photosynthetic Bacterial Reaction Center II, Plenum Press, New York, 1992, pp. 363–374.
[50] P. Maróti, C.A. Wraight, Biophys. J. 73 (1997) 367–381.
[51] C.R. Lancaster, H. Michel, Structure 5 (1997) 1339–1359.
[52] A.K. Grafton, R.A. Wheeler, J. Phys. Chem. 103 (1999) 5380–5387.
[53] E. Takahashi, C.A. Wraight, Biochemistry 31 (1992) 855–866.
[54] W.F. Butler, R. Calvo, D.R. Fredkin, R.A. Isaacson, M.Y. Okamura, G. Feher, Biophys. J. 45 (1984) 947–973.
[55] R.C. Prince, P.L. Dutton, Arch. Biochem. Biophys. 172 (1976) 329–334.
[56] P. Beroza, D.R. Fredkin, M.Y. Okamura, G. Feher, Biophys. J. 68 (1995) 2233–2250.
[57] C.R. Lancaster, H. Michel, B. Honig, M.R. Gunner, Biophys. J. 70 (1996) 2469–2492.
[58] R.I. Cukier, D.G. Nocera, Annu. Rev. Phys. Chem. 49 (1998) 337–369.
[59] M. Paddock, M. Graige, G. Feher, M. Okamura, Biophys. J. 74 (1998) A135.
[60] M.S. Graige, M.L. Paddock, G. Feher, M.Y. Okamura, Biochemistry 38 (1999) 11465–11473.
[61] J.F. Nagle, S. Tristram-Nagle, J. Membr. Biol. 74 (1983) 1–14.
[62] E. Takahashi, C.A. Wraight, Biochim. Biophys. Acta 1020 (1990) 107–111.
[63] M.L. Paddock, S.H. Rongey, P.H. McPherson, G. Feher, M.Y. Okamura, Biophys. J. 59 (1991) 142a.
[64] M.L. Paddock, S.H. Rongey, P.H. McPherson, A. Juth, G. Feher, M.Y. Okamura, Biochemistry 33 (1994) 734–745.
[65] M.L. Paddock, P.H. McPherson, G. Feher, M.Y. Okamura, Proc. Natl. Acad. Sci. USA 87 (1990) 6803–6807.
[66] W. Leibl, I. Sinning, G. Ewald, H. Michel, J. Breton, Biochemistry 32 (1993) 1958–1964.
[67] M.L. Paddock, G. Feher, M.Y. Okamura, Biochemistry 34 (1995) 15742–15750.
[68] M.L. Paddock, M.E. Senft, M.S. Graige, S.H. Rongey, T. Turanchik, G. Feher, M.Y. Okamura, Photosynth. Res. 55 (1998) 281–291.
[69] M. Paddock, G. Feher, M. Okamura, Biophys. J. 68 (1995) A246.
[70] M.L. Paddock, A. Juth, G. Feher, M.Y. Okamura, Biophys. J. 61 (1992) 101a.
[71] E. Takahashi, C.A. Wraight, Proc. Natl. Acad. Sci. USA 93 (1996) 2640–2645.
[72] M.L. Paddock, S.H. Rongey, G. Feher, M.Y. Okamura, Proc. Natl. Acad. Sci. USA 86 (1989) 6602–6606.
[73] P.H. McPherson, M. Schönfeld, M.L. Paddock, M.Y. Okamura, G. Feher, Biochemistry 33 (1994) 1181–1193.
[74] V.P. Shinkarev, E. Takahashi, C.A. Wraight, Biochim. Biophys. Acta 1142 (1993) 214–216.
[75] H. Michel, K.A. Weyer, H. Gruenberg, I. Dunger, D. Oesterhelt, F. Lottspeich, EMBO J. 5 (1986) 1149–1158.
[76] S.H. Rongey, M.L. Paddock, G. Feher, M.Y. Okamura, Proc. Natl. Acad. Sci. USA 90 (1993) 1325–1329.
[77] D.K. Hanson, S.L. Nance, M. Schiffer, Photosynth. Res. 32 (1992) 147–153.
[78] D.K. Hanson, L. Baciou, D.M. Tiede, S.L. Nance, M. Schiffer, P. Sebban, Biochim. Biophys. Acta 1102 (1992) 260–265.
[79] D.K. Hanson, D.M. Tiede, S.L. Nance, C.H. Chang, M. Schiffer, Proc. Natl. Acad. Sci. USA 90 (1993) 8929–8933.
[80] P. Maróti, D.K. Hanson, L. Baciou, M. Schiffer, P. Sebban, Proc. Natl. Acad. Sci. USA 91 (1994) 5617–5621.
[81] J. Miksovska, L. Kálmán, M. Schiffer, P. Maróti, P. Sebban, D.K. Hanson, Biochemistry 36 (1997) 12216–12226.
[82] J. Miksovska, M. Valerio-Lepiniec, M. Schiffer, D.K. Hanson, P. Sebban, Biochemistry 37 (1998) 2077–2083.
[83] M. Schiffer, C.-K. Chan, C.-H. Chang, T.J. DiMagno, G.R. Fleming, S. Nance, J. Norris, S. Snyder, M. Thurnauer, D.M. Tiede, D.K. Hanson, in: J. Breton, A. Vermeglio (Eds.), The Photosynthetic Bacterial Reaction Center II, Plenum Press, New York, 1992, pp. 351–361.
[84] P. Sebban, P. Maróti, M. Schiffer, D.K. Hanson, Biochemistry 34 (1995) 8390–8397.
[85] M. Valerio-Lepiniec, J.D. Delcroix, M. Schiffer, D.K. Hanson, P. Sebban, FEBS Lett. 407 (1997) 159–163.
[86] M. Valerio-Lepiniec, J. Miksovska, M. Schiffer, D.K. Hanson, P. Sebban, Biochemistry 38 (1999) 390–398.
[87] M.Y. Okamura, M.L. Paddock, P.H. McPherson, S. Rongey, G. Feher, in: N. Murata (Ed.), Research in Photosynthesis, Kluwer Academic Publishers, Dordrecht, 1992, pp. 349–356.
[88] M.L. Paddock, H.L. Axelrod, E.C. Abresch, A.P. Yeh, D.C. Rees, G. Feher, M.Y. Okamura, Biophys. J. 76 (1999) A141.
[89] E. Nabedryk, J. Breton, M.Y. Okamura, M. Paddock, Photosynth. Res. 55 (1998) 293–299.
[90] M.R. Gunner, B. Honig, in: J. Breton, A. Vermeglio (Eds.), The Photosynthetic Bacterial Reaction Center II, Plenum Press, New York, 1992, pp. 403–410.
[91] B. Rabenstein, G.M. Ullmann, E.W. Knapp, Biochemistry 37 (1998) 2488–2495.
[92] J. Breton, E. Nabedryk, C. Mioskowski, C. Boullais, in: M.-E. Michel-Beyerle (Ed.), The Reaction Center of Photosynthetic Bacteria, Structure and Dynamics, Springer-Verlag, New York, 1996, pp. 381–394.
[93] G. Zundel, Trends Phys. Chem. 3 (1992) 129–156.
[94] J. le Coutre, J. Tittor, D. Oesterhelt, K. Gerwert, Proc. Natl. Acad. Sci. USA 92 (1995) 4962–4966.
[95] J. Breton, E. Nabedryk, Photosynth. Res. 55 (1998) 301–307.
[96] Y.Y. Sham, I. Muegge, A. Warshel, Proteins 36 (1999) 484–500.
[97] H.L. Axelrod, E.C. Abresch, M.L. Paddock, M.Y. Okamura, G. Feher, Proc. Natl. Acad. Sci. USA 97 (2000) 1542–1547.
[98] M.L. Paddock, G. Feher, M.Y. Okamura, Proc. Natl. Acad. Sci. USA 97 (2000) 1548–1553.
[99] J.T. Beatty, M.L. Paddock, M.Y. Okamura, Biophys. J. 78 (2000) 339A.